How to cite: *Angew. Chem. Int. Ed.* **2022,** *61,* e202204611
International Edition: doi.org/10.1002/anie.202204611
German Edition: doi.org/10.1002/ange.202204611

Supramolecular Chemistry

# Small-Molecule-based Supramolecular Plastics Mediated by Liquid-Liquid Phase Separation**

*Jingjing Yu, Dawei Qi, Ermei Mäkilä, Lippo Lassila, Anastassios C. Papageorgiou, Markus Peurla, Jessica M. Rosenholm, Zhao Zhao, Pekka Vallittu, Sirpa Jalkanen, Chunman Jia, and Jianwei Li**

**Abstract:** Plastics are one of the most widely used polymeric materials. However, they are often undegradable and non-recyclable due to the very stable covalent bonds of macromolecules, causing environmental pollution and health problems. Here, we report that liquid-liquid phase separation (LLPS) could drive the formation of robust, stable, and sustainable plastics using small molecules. The LLPS process could sequester and concentrate solutes, strengthen the non-covalent association between molecules and produce a bulk material whose property was highly related to the encapsulated water amounts. It was a robust plastic with a remarkable Young's modulus of 139.5 MPa when the water content was low while became adhesive and could instantly self-heal with more absorbed water. Finally, responsiveness enabled the material to be highly recyclable. This work allowed us to understand the LLPS at the molecular level and demonstrated that LLPS is a promising approach to exploring eco-friendly supramolecular plastics that are potential substitutes for conventional polymers.

## Introduction

Plastics are one of the most widely used polymeric materials that are of low cost and highly efficient for manufacturing daily products. However, plastics are often difficult to degrade or recycle due to the very stable covalent bonds of macromolecules, leading to environmental pollution and health problems.[1] To tackle the long-standing challenge to humans from plastics, small molecule-based supramolecular polymers have been proposed to replace conventional polymers.[2–5] Unfortunately, there are huge challenges to improve the mechanical property and plasticity of small molecule-based supramolecular polymers, thus impeding their applications in practice.[6,7] Such unsatisfactory developments arise from the labile noncovalent bonding between small molecules for supramolecular polymerization. The bond strength of noncovalent interactions is weak, and solvent molecules can interfere with the bonding between solutes, always resulting in a low degree of supramolecular polymerization.[8,9] Keeping these aspects in mind, we propose achieving robust supramolecular plastics by designing small self-assemblers with various potential binding

[*] Dr. J. Yu, D. Qi, Dr. Z. Zhao, Dr. S. Jalkanen, Dr. J. Li
MediCity Research Laboratory, University of Turku
Tykistökatu 6, 20520 Turku (Finland)
E-mail: jianwei.li@utu.fi

Dr. E. Mäkilä
Laboratory of Industrial Physics, Department of Physics and Astronomy, Institute of Dentistry, University of Turku
20014 Turku (Finland)

Dr. L. Lassila, Prof. Dr. P. Vallittu
Department of Biomaterials Science and Turku Clinical Biomaterials Centre, TCBC, University of Turku
20014 Turku (Finland)

Prof. Dr. A. C. Papageorgiou
Turku Bioscience Centre, University of Turku
20521 Turku (Finland)
and
Turku Bioscience Centre, Åbo Akademi University
20521 Turku (Finland)

Dr. M. Peurla
Institute of Biomedicine and FICAN West Cancer Research Laboratories, University of Turku
20014 Turku (Finland)

Prof. Dr. J. M. Rosenholm
Pharmaceutical Sciences Laboratory, Faculty of Science and Engineering, Åbo Akademi University
Tykistökatu 6, 20520 Turku (Finland)

Prof. Dr. P. Vallittu
City of Turku Welfare Division
Puolalankatu 5, 20101 Turku (Finland)

Prof. Dr. C. Jia, Dr. J. Li
Hainan Provincial Key Laboratory of Fine Chem, School of Chemical Engineering and Technology, Hainan University
570228 Haikou (China)
and
One Health Institute, Hainan University
570228 Haikou (China)

[**] A previous version of this manuscript has been deposited on a preprint server (https://doi.org/10.26434/chemrxiv-2022-snwcn).

moieties and developing strategies to increase the concentration density of the self-assemblers. Multiple binding sites are beneficial for strengthening the intermolecular association affinity for polymerization through multivalence effects.[10] A high concentration density would reduce the side effects from solvent molecules.

Liquid-liquid phase separation (LLPS) is a process where a dense phase forms from a dilute phase at thermodynamic equilibrium.[11–13] The formation of the dense phase is directed by intermolecular noncovalent interactions, giving rise to stable compartments in solution that sequester and concentrate solutes. In contrast to the formation process of supramolecular materials such as micelles, vesicles and fibres,[14] LLPS can produce larger aggregates—micrometre-scale droplets in solution that can even grow into macroscopic materials consisting of solutes with a high concentration density.[15,16]

Here, we demonstrate that LLPS can be a powerful strategy to explore supramolecular plastics using phase-segregating ionic complexes consisting of cationic charged macrocycles and countercharged surfactants. The small molecule-based material is named a macrocycle-surfactant phase separated (MSPS) material (Scheme 1). The property of the MSPS material was highly related to water content. With a saturated water content, the material was like a fluid and could self-heal instantly even underwater and showed top-of-the-range waterproof adhesiveness in terms of materials made from small molecules. By reducing water molecules, the MSPS material (sol) showed a transition to a gel with mechanical properties comparable to those of covalent polymers. Moreover, the photoreversibility and thermoreversibility and simultaneous stability equipped the material with excellent processability and usability. Finally, the redox-sensitive disulfide bonds in the macrocycle made the materials degradable and highly recyclable. These findings suggest that LLPS represents an effective and powerful strategy for constructing robust bulk supramolecular materials with adhesive properties without compromising the responsiveness and offers an approach for exploring eco-friendly materials that could potentially be substitutes for conventional covalent polymers.

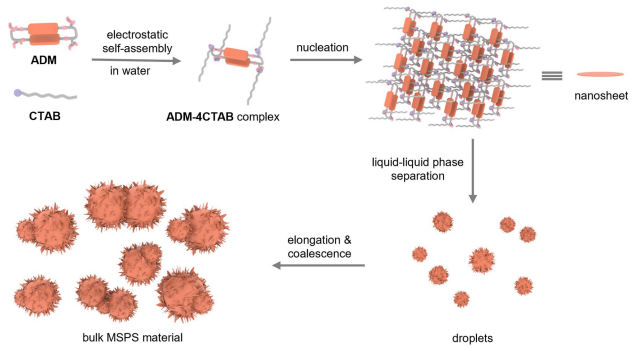


***Scheme 1.*** Illustration of molecular mechanism for the formation of MSPS materials that were self-assembled by **ADM** macrocycles and **CTAB** surfactants in water.

## *Results and Discussion*

In our previous work, an azobenzene-derived macrocycle (**ADM**) linked by disulfide bonds was screened from a dynamic combinatorial library by a highly selective gelation process with magnesium cations ($Mg^{2+}$).[17] Apart from the electrostatic interaction, the gelation benefited from multiple noncovalent interactions including π-π stacking between the azobenzene moieties, hydrogen bonding between the amide NH group and carboxylate groups and bridged water interactions between the amide carbonyl or carboxylate group. Encouraged by this successful example of engineering various types of noncovalent interactions in a single molecule to explore supramolecular materials, we regarded **ADM** as an ideal candidate for LLPS because the repeating units in the macrocycle could multiply the number of noncovalent interactions. Together with **ADM**, the small cationic surfactant cetyltrimethylammonium bromide (**CTAB**) was chosen to verify small molecule-based LLPS[18] (Figure 1a).

A group of aqueous solution at pH 10 was prepared from **ADM** at the same concentration (10 mM) and **CTAB** at various concentrations with mole ratios. When the solution was mixed with **ADM** (*x* mM) and **CTAB** at a mole ratio of 1 : n, the name of the solution was **ADM** (*x* mM)/**CTAB**/1 : n. The solution **ADM** (10 mM)/**CTAB**/1 : 4 was homogeneously turbid at the beginning when it was made. Interestingly, a clear and sticky soft material was obtained as a separated phase from the water solution after three hours (Figure S1). To gain insights into the formation of the material, time-lapse microscopy was first used to monitor the growth process with time (Figure 1b, S2, Movie S1). In an early stage after mixing, small round droplets with a diameter of approximately 1 μm appeared gradually. Thereafter, the diameter of the droplets increased to approximately 20 μm. Then, the growth kinetics of the droplets prior to full phase separation were investigated using dynamic light scattering (DLS) (Figure 1c). The sigmoidal profile of the increase in diameter overtime was consistent with the typical size growth of MSPS materials.[19,20]

The LLPS in solution containing **ADM** (10 mM) and **CTAB** at the other ratios was also checked using time-lapse microscopy. MSPS materials were observed only in the **ADM** (10 mM)/**CTAB**/1 : 3 solution, but their phase separation was not as obvious as that in the **ADM** (10 mM)/**CTAB**/1 : 4 solution (Figure S3). The zeta potential of the MSPS materialssuggested a neutral charge (Figure S4). These results suggest that the stoichiometric ratio was the optimized condition for complex LLPS, as it featured a neutral charge stoichiometry, which was consistent with most oppositely charged complex LLPS.[21,22]

To determine the microstructures in the MSPS materials, we lyophilized the condensed phase that was isolated from the solution and analyzed the morphology of the bulk material using field-emission scanning electronic microscopy (FE-SEM). The surface of the material was attached to nanosheets approximately 100 nm in width and 500 nm to 1000 nm in length (Figure S5). By using atomic force microscope (AFM), the average thickness of the nanosheets was

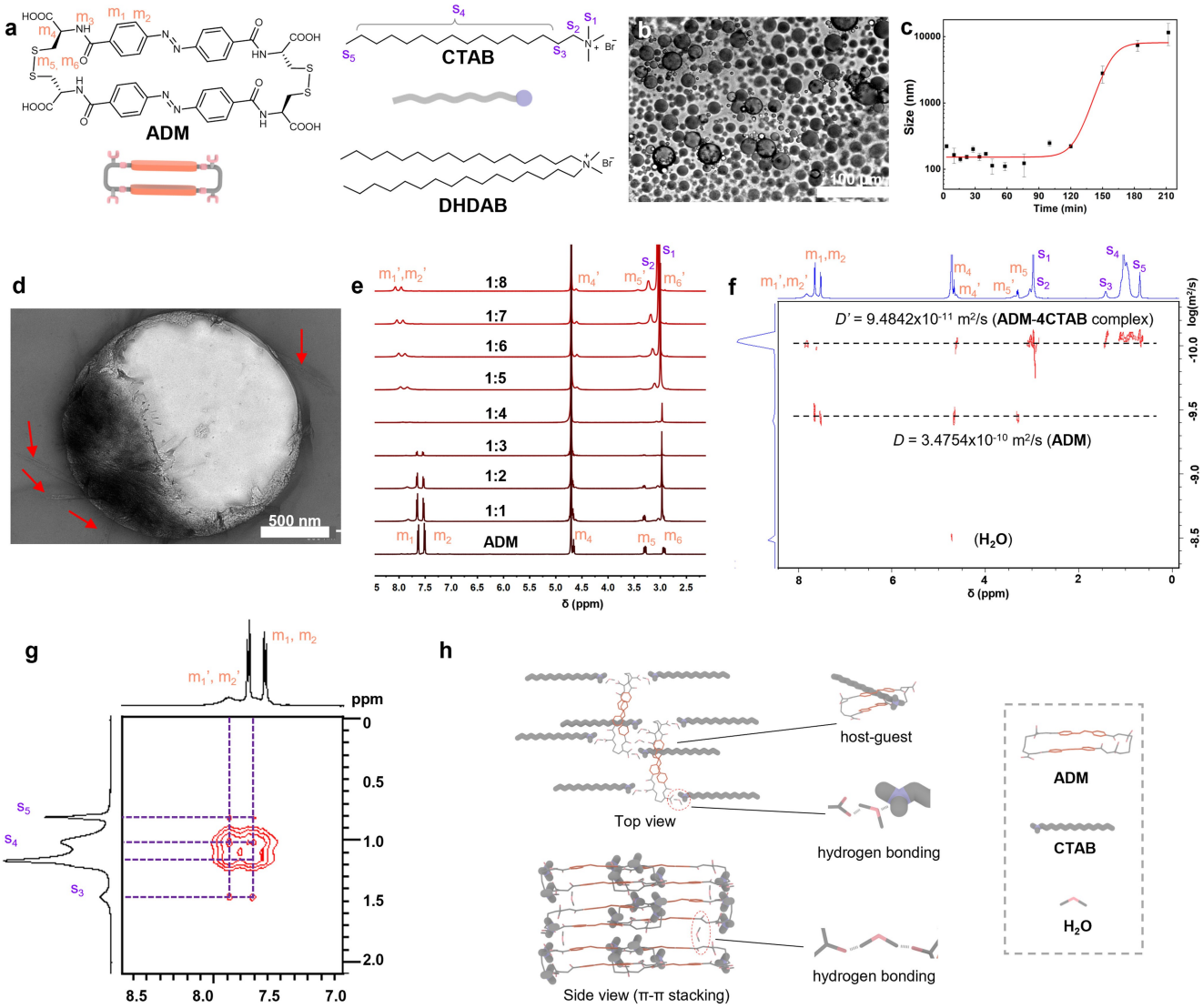


***Figure 1.*** a) Chemical structures of **ADM** macrocycle, **CTAB** and **DHDAB** surfactants. b) Time-lapse bright field microscopy images of **ADM** (1 mM)/**CTAB**/1 : 4 mixture at 90 min after solution preparation. c) Evolution of the average size of droplets with time before full phase separation in **ADM** (0.1 mM)/**CTAB**/1 : 4 solution. (pH ≈ 10, $H_2O$). d) TEM image of samples taken from **ADM** (1 mM)/**CTAB**/1 : 4 mixture at 15 min after solution preparation (inserted red arrow: nanosheets). e) Partial $^1$H NMR spectra of **ADM** (10 mM)/**CTAB**/1 : n. (pD ≈ 10, $D_2O$, 500 MHz). f) DOSY spectrum of **ADM** (10 mM)/**CTAB**/1 : 2. (pD ≈ 10, $D_2O$, 600 MHz). g) Partial 2D NOESY spectra of **ADM** (10 mM)/**CTAB**/1 : 2. (pD ≈ 10, $D_2O$, 600 MHz, the mixing time: 100 ms and relaxation delay: 2 s). h) Chemical structure illustration of interwoven **ADM-4CTAB** MSPS materials in top view and side view, zoom-in pictures show the details of host–guest and hydrogen bonding interaction between carboxylic groups, amide bonds and water molecules.

measured as approximately 40 nm (Figure S6). These results suggest that the droplets could be organized by the nanosheets. This inference was further verified by examining the detailed morphological evolution of the droplets using transmission electron microscopy (TEM). Samples for the analysis were taken at 5 min, 15 min and 120 min after the solution (pH 10) **ADM** (0.1 mM)/**CTAB**/1 : 4 was prepared. Thin nanosheets were observed in the early stage (Figure S7a). Subsequently, small droplets appeared with the nanosheets on their surfaces (Figure 1d), which was consistent with the FE-SEM analysis. Over time, the small droplets fused into larger droplets with a diameter of approximately 15 μm (Figure S7b), which was similar to the size of droplets observed by time-lapse microscopy at 120 min after the solution had been made. Thus, we inferred that the three-dimensional MSPS droplets were grown from two-dimensional nanosheets (Scheme 1).

We proceeded to study the organization of the MSPS materials at the molecular level. The composition of the lyophilized material was first identified using proton nuclear magnetic resonance ($^1$H NMR) in $CD_3OD$. The integration of proton signals confirmed that the MSPS materials were formed by **ADM** and **CTAB** with a mole ratio of 1 : 4 (Figure S8). The resulting complex was denoted as **ADM**:4**CTAB**. Unfortunately, it was not feasible to study further the molecular interaction between the **ADM**:4**C-**

**TAB** complexes in the **ADM**/**CTAB**/1:4 solution using NMR technology owing to the excessively diluted concentration in $D_2O$ resulting from liquid-liquid phase separation (see Figure 1e). Noting that solution prepared from **ADM** and **CTAB** with ratios other than 1:3 and 1:4 were homogeneous, we first recorded a group of $^1H$ NMR spectra for the solution **ADM** (10 mM)/**CTAB**/1:n in $D_2O$ (pD 10) (see Figure 1e). With the increase of **CTAB** into the solution of **ADM**, the peak area of **ADM** gradually decreased, accompanied by the appearance of new broad peaks at 7.9 ppm and at 7.7 ppm which should be assigned to the protons $m_1$ and $m_2$ of the azobenzene moiety, respectively. The proton signals ($m_4$, $m_5$ and $m_6$) of the cysteine moieties in **ADM** exhibited similar shifting behaviours. All the original sharp peaks of protons at **ADM** were finally replaced by new broad peaks after the mixing ratio of **ADM** and **CTAB** was over 1:4. We assumed that the newly appeared broad peaks were from the aggregates of the complex **ADM**:4**CTAB**.

To verify this assumption, we then analysed the solution **ADM** (10 mM)/**CTAB**/1:2 in $D_2O$ (pD 10) using diffusion ordered spectroscopy (DOSY). The plot of the solution **ADM** (10 mM)/**CTAB**/1:2 in $D_2O$ (pD 10) showed only two types of aggregates due to their distinguishable diffusion coefficients.[23] The proton signals $m_{1'}$ and $m_{2'}$ assigned to the azobenzene moiety shared the same diffusion coefficient ($D' = 9.4842 \times 10^{-11}\ m^2 s^{-1}$) with protons $s_1$, $s_2$, $s_3$, and d from the alkyl chain of **CTAB**, suggesting that the **ADM**:4**CTAB** complex was formed and further piled into large aggregates (Figure 1f). The other type of aggregates was formed by pure **ADM**, as the protons corresponding to **ADM** had a diffusion coefficient ($D = 3.4754 \times 10^{-10}\ m^2 s^{-1}$) similar to that of aggregates in solution prepared from only **ADM** ($D = 3.7934 \times 10^{-10}\ m^2 s^{-1}$) (Figure S9). To understand the interaction between the complex **ADM**:4**CTAB**, we also analysed the solution **ADM** (10.0 mM)/**CTAB**/1:2 and 1:6 in $D_2O$ (pD 10.0) using two-dimensional nuclear Overhauser effect spectroscopy (NOESY) (Figure 1g, S10, S11). There were strong nuclear Overhauser effects (NOEs) between protons $m_{1'}$ and $m_{2'}$ from the newly formed broad peaks of azobenzene moieties and protons $s_1$, $s_2$, $s_3$, and $s_4$ from the alkyl chain of **CTAB**, while no obvious NOEs were observed between protons $m_1$ and $m_2$ from **ADM** and the alkyl chain protons of **CTAB**. This result demonstrated that the alkyl chain of **CTAB** interpenetrated the **ADM** macrocycle, giving rise to pseudorotaxane-like substructures for the subsequent formation of supramolecular polymers[9,24] (Figure 1h).

Previously, we obtained single-crystal structures of **ADM** coordinated with $Ca^{2+}$. The spacings of azobenzene units within the **ADM** and between two adjacent macrocycles were represented by two typical distances of 3.3 Å and 3.6 Å, respectively.[17] Indeed, the analysis of the powder XRD data of the lyophilized MSPS materials (Figure S12) revealed two distances for π-π interactions that were 3.98 Å and 4.19 Å. The longer distances may be attributed to the interpenetration of the alkyl chain of **CTAB** into the **ADM** macrocycle.

In addition to π-π interactions, the LLPS process for the formation of MSPS materials cannot take place without the involvement of water molecules.[13,25] To understand the role of water molecules in the **ADM-4CTAB** MSPS materials, we first investigated the hydration and dehydration behaviour of the material (Figure S13). The maximum percentage of water content in the **ADM-4CTAB** MSPS materials was determined to be approximately 45 %. The fully hydrated material could be dehydrated in air, and the percentage of water could be minimized to approximately 5 %. Water states of MSPS materials could be further investigated by thermogravimetric analysis (TGA) and differential scanning calorimeter (DSC)[26–28] (Figure S14–16, Table S1), two distinguished water states including non-freezable (bound) and freezable (free) water could be calculated out (Figure S16). With the increase of the total amounts of water in the material, the non-freezable water content experienced a linear growth to reach a saturated value around 17 %. During the stage of the linear growth, the amounts of the freezable water were negligible, as most of the water was non-freezable. These results indicated that water molecules involved in the formation of the MSPS materials and hydrogen bonding formed at the hydrophilic sites of the complex **ADM**:4**CTAB**.

The role of water molecules in hydrogen bonding was further investigated using attenuated total reflectance-Fourier transform infrared (ATR-FTIR) spectroscopy. ATR-FTIR tests were carried out on the **ADM-4CTAB** MSPS materials without water and with 5.6 % water content (Figure S17). To avoid the overlap of the O–H band of water with the hydrogen bonds in the MSPS materials, we prepared the samples in deuterated water ($D_2O$) solution.[29] The initial broad peak at 3368 $cm^{-1}$ in the ATR-FTIR spectrum of the lyophilized MSPS material represents the N–H bond stretching vibration ($\upsilon_s$ N–H) of the amide group of **ADM**. It shifted to 3380 $cm^{-1}$ in the presence of $D_2O$, which was attributed to the fact that the addition of $D_2O$ promoted the gradual exchange of N–H bonds to N–D bonds and the formation of hydrogen bonds between $D_2O$ and N-D.[30] In addition, the peak at 1650 $cm^{-1}$ assigned to the C=O stretching of the amid group shifted to 1643 $cm^{-1}$. This wavenumber downshift was due to hydrogen bonding between the carbonyl group of the amid and $D_2O$. However, the peak at 1370 $cm^{-1}$ assigned to the C=O symmetric stretching vibration of the carboxylate group was shifted by +7 $cm^{-1}$, which was induced by the coordination between the oxygen of $D_2O$ and the ammonium salt. These results suggested that water molecules bridged interactions between amide carbonyl or carboxylate groups and the ammonium salt, which was similarly observed in the crystal formed by **ADM** and $Ca^{2+}$.[17]

Taken together, the MSPS materials were assembled under the direction of multiple noncovalent interactions (Figure 1h). The MSPS materials were organized by the **ADM**:4**CTAB** complex that was formed through ionic interactions. As the overall charge of the complex was nearly zero, the complex was generally hydrophobic. Due to hydrophobic effects, the alkyl tail of **CTAB** was buried in the hydrophobic cavity of the **ADM** macrocycle, resulting in

the formation of a pseudorotaxane-like substructure for supramolecular polymerization into two-dimensional structures. In addition, through hydrogen bonding, water molecules bridged the interaction of macrocycles, helping and aligning the π-π stacking of the azobenzene moieties. The cooperation of these noncovalent interactions led to the aggregation of the two-dimensional structure into a dense phase and pushed most water molecules into the diluted phase, giving rise to three-dimensional droplets (Scheme 1).

We have shown that MSPS materials could be reversibly hydrated and dehydrated. By absorbing water, the **ADM-4CTAB** materials became viscous from elastic. This change was clarified by studying the viscoelasticity of the material with various water contents using a rheometer. Firstly, the transition from a viscoelastic hydrogel to a viscoelastic fluid during the hydration process was confirmed by strain sweep measurements (Figure 2a). All the tested **ADM-4CTAB** materials had strain ranges where both storage modulus (G′) and loss modulus (G″) remained constant, which was defined as strain-defined linear viscosity (LVE) regions. In the LVE region, the structure of the sample was not destroyed when the tests were performed. For the material with the water content ≈5 %, the G′ representing elasticity was 10 times larger than the G″ representing viscosity in the LVE region, indicating the sample was a typical semi-solid material with a stable gelling state. With the increase of water content to approximately 20 %, the G′ decreased significantly and became nearly identical to G″, revealing the transition point of semi-solid to semi-fluid. When the water content in the material reached to approximately 45 %, the G′ was smaller than the G″, which is the feature of a viscoelastic fluid.

Considering the dynamics of the non-covalent interactions and molecular conformations for the formation of the **ADM-4CTAB** materials, we reasoned that the mechanical property should be time-relevant. Then, the viscoelasticity of the **ADM-4CTAB** materials in different time scales were further tested by frequency sweep measurements (Figure 2b). For the material with a water content approximately 5 %, the G′ and G″ were not significantly affected by the change of frequency. However, with the increase of water contents in the materials to approximately 20 % and 45 %, both moduli declined as the decrease of frequency while G′ was declining in a steeper slope than G″. This suggested that water molecules enabled the **ADM-4CTAB** materials to dissipate more energy input in the prolonged timescale. Interestingly, the descending slope was even steeper for the **ADM-4CTAB** materials with 45 % of water, which could be explained by the sticky rouse polymer dynamics.[31] The additional water enhanced the mobility of the molecular assemblies in the MSPS materials by competing or dispersing the supramolecular interactions. These results indicated that the water content could effectively regulate the time-relevant viscoelasticity of the **ADM-4CTAB** material from stable semi-solids to dissipative semi-solids/fluids.

The fluidic properties of the **ADM-4CTAB** MSPS materials with saturated water content were further evaluated by checking its dynamic viscosity (Figure 2c). The viscosity of the material decreased while the shear rate increased, exhibiting shear thinning behaviour. This non-Newtonian behaviour usually occurs in solution of polymers due to the breaking of the physical cross-links between macromolecules under the action of shearing force.[31,32] However, such behaviour shown in the small molecule-based fluidic material suggested that physical cross-linked networks also formed in the MSPS material, which probably resulted from the pseudorotaxane substructure. Subsequently, to test the resilience of the physical network, the thixotropy of the material was investigated by cyclic strain sweep (Figure 2d, S18). The materials were yielded at a strain out of the linear viscoelastic region, showing a dramatic drop of both G′ and G″. After going back to a strain in the linear viscoelastic region, an instant recovery of materials' strength was shown, which was a common feature of the materials with reversible non-covalent crosslinks. However, the recovery was not 100 % reversible in the tested time region, especially for the first cycle. This loss could be attributed to the disentanglement of the molecular assemblies requiring much longer time to reform.[31] Encouraged by the recovery ability of the physical network, we inferred that the material should also be self-healable. Indeed, several pieces of the material cut by a knife automatically self-healed instantly both underwater and in the air without any other treatment (Figure 3a, Movie S2). The tensile-stress tests on the self-healed material indicated that 82 % of the fracture strength could be recovered (Figure S23).

Complex MSPS materials formed by oppositely charged polyelectrolytes have been proven to be ideal adhesives due to their fluid state, water immiscibility and high density.[15,16] However, the adhesiveness of small molecule-based MSPS materials has rarely been studied. Here, the adhesive properties of **ADM-4CTAB** MSPS materials containing 45 % water were tested at the interfaces of various substrates (Figure 3b, c, S19). Due to the high-density

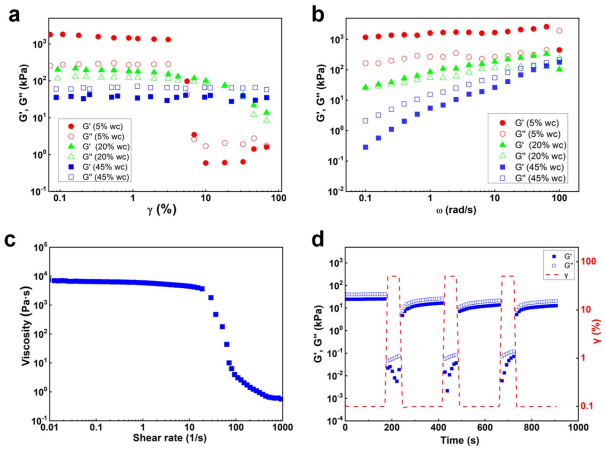


***Figure 2.*** a) Strain sweeps and b) frequency sweeps showing loss (G″, open data point) and storage moduli (G′, filled data points) of bulk **ADM-4CTAB** MSPS materials with ≈5 %, ≈20 % and ≈45 % water content. c) Shear-viscosity tests of **ADM-4CTAB** MSPS materials with ≈45 % water content. d) Cyclic strain sweep of **ADM-4CTAB** MSPS materials with ≈45 % water content.

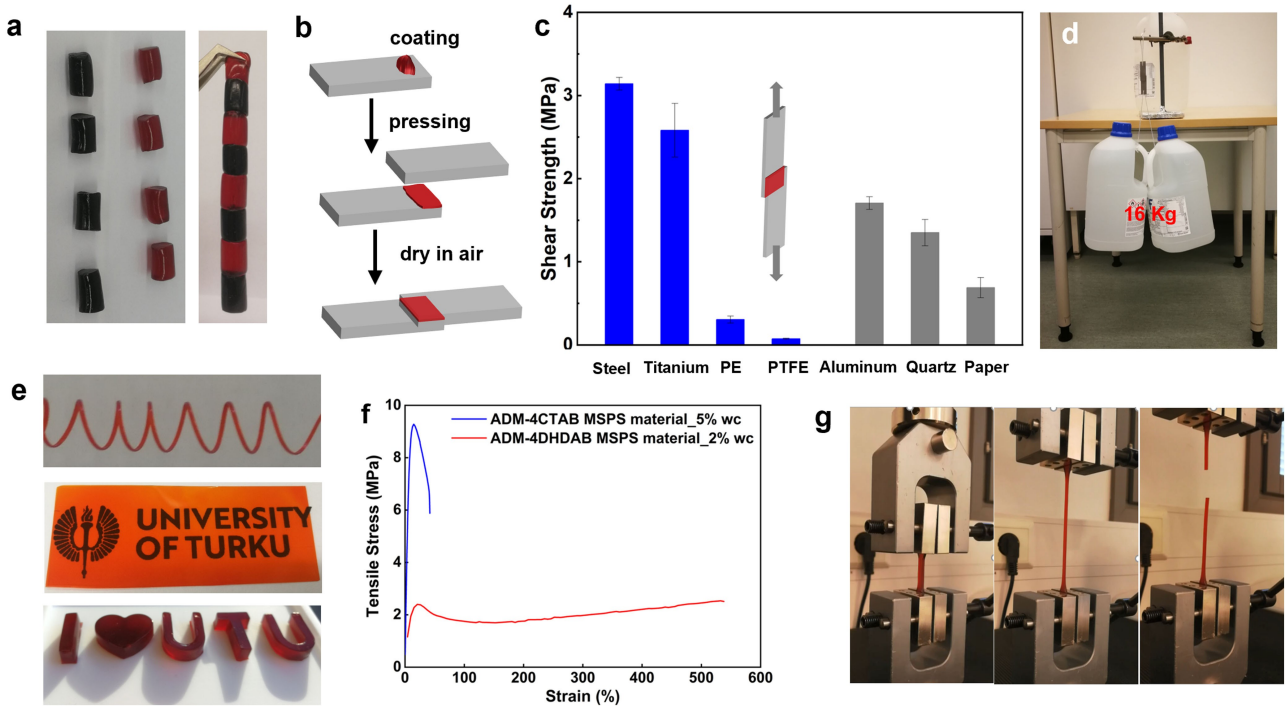


***Figure 3.*** a) Photograph of cylinder-like **ADM-4CTAB** MSPS materials specimens after cutting into several fragments and subsequent self-healing process (dark bule specimen was colored by Brilliant blue R-250). b) Brief schematic illustration of lap-shear specimen preparation of **ADM-4CTAB** MSPS materials. c) The lap-shear strength of **ADM-4CTAB** MSPS materials apply for different substrates (gray bar indicated the substrate plates have been broke before pulled apart). d) Photographs of macroscopic adhesive behavior of **ADM-4CTAB** MSPS materials applied to steel substrates. e) Photograph of free-standing **ADM-4CTAB** MSPS materials after processing into specific shapes (bottom to up: art words, transparent film, spring). f) Tensile-stress curves of free-standing **ADM-4CTAB** (≈5% wc) MSPS materials and **ADM-4DHDAB** MSPS materials (≈2% wc). g) Photograph of free-standing **ADM-4DHDAB** MSPS materials after elongation and fracture.

hydrogen bonding interactions in the **ADM-4CTAB** MSPS materials, the material showed high adhesive strength to hydrophilic surfaces, but the strength was weaker on hydrophobic surfaces. The adhesiveness of the material was quantified by determining the shear strength up to 3.1 ± 0.1 MPa using the specimens with steel substrates. This value was higher than or comparable to most previously reported supramolecular polymer adhesives.[29,33–35] The joint specimens made of steel could hold a 16 kg weight over a month (Figure 3d, Movie S3). Furthermore, the adhesive strength could be weakened to 1.6 ± 0.1 MPa after immersion in water for 12 hours (Figure S20), but it was still within the top value range for supramolecular adhesives.[33,36]

Finally, the robustness of the dehydrated material was studied. The aforementioned strain sweep measurements of the **ADM-4CTAB** MSPS materials containing 5% water dehydrated from 45% demonstrated that the material was a hydrogel. A closer inspection of the data revealed that the storage modulus of the material was over a million Pa. In addition, as shown in Figure 3e, the **ADM-4CTAB** MSPS materials with ≈5% water content showed ease of processing, as they could be transformed into free-standing objectives with various shapes at room temperature. These results encouraged us to further test the mechanical properties of the material. The tensile-stress test suggested that the **ADM-4CTAB** MSPS materials with ≈5% water content had a remarkable Young's modulus, 139.5 MPa, and a tensile strength of 9.2 MPa (Figure 3f). However, it showed a maximum fracture elongation of 40%. To improve its stretchability, a similar gel was prepared from the same macrocycle **ADM** and a cationic surfactant dihexadecyldimethylammonium bromide (**DHDAB**) with two alkyl chains under the same experimental conditions (Figure 1a). Unlike the aforementioned **ADM-4CTAB** MSPS materials, the maximum water content of the MSPS materials made from **ADM** and **DHDAB** was only ≈18%, while the dehydration curve in air showed that the residue water content was ≈2% (Figure S21), and the material exhibited different rheological properties as well (Figure S22). The elongation at break of the free-standing **DHDAB**-based materials with 2% water was increased to 528% (Figure 3f, g, Movie S4). These results illustrated that the dehydrated MSPS material was robust, showing mechanical properties comparable to those of macromolecular polymers,[37,38] even though it was built from small molecules without covalent crosslinkers. By tuning the hydrophobicity of the surfactant, we could control the elongation property of the resulting MSPS materials.

The proven robustness and ease of processing of MSPS materials should allow us to extend their practical applications as non-covalent polymers. However, the new materials should be stable yet degradable and recyclable. The stability of the material was first evaluated by monitoring the leakage content of the **ADM-4CTAB** MSPS materials in distilled

water at room temperature and under harsh conditions, i.e., in a solution of phosphate buffered saline (PBS, 1×, pH 7.4) at 37 °C (Figure 4a). The material was extremely stable in distilled water but partially dissolved in PBS buffer solution at 37 °C after 5 days. This was probably because the ionic interaction between the **ADM** macrocycle and the surfactants was weakened by the buffer salts.[39] However, the stability of the material could be improved by introducing more hydrophobic moieties into the cationic surfactant. The MSPS material made from **ADM** and **DHDAB** had only 1.5 % leakage into PBS buffer at 37 °C even after immersion for 15 days. Then, the photostability of the bulk material was tested since the *trans* form of the azobenzene units in the **ADM** macrocycle could be isomerized to the *cis* form under UV light at 365 nm (Figure S24), which further induced the disassembly of the **ADM-4CTAB** MSPS droplets[19,40] (Figure 4b–d). However, no obvious morphological changes of the bulk **ADM-4CTAB** materials were observed after UV irradiation. Finally, MSPS materials are thermosensitive due to the massive hydrogen bonding interactions according to the temperature-variable rheological properties (Figure S25), but the structure showed good thermostability under heating (100 °C) and cooling cycles (−55 °C) according to the DSC plots (Figure S15). There were upper-critical solution temperatures (UCST) in the **ADM-4CTAB** MSPS materials, which were ≈45 °C and ≈27 °C for the materials with ≈5 % and 20 % water contents, respectively (Figure S25). When bulk **ADM-4CTAB** MSPS materials were evaluated by cyclic temperature sweep (Figure 4e, S26), the phase transition of the material was proven fully reversible. The mechanical modulus could be fully recovered under at least three heating-cooling cycles. The reversible UCST phase transition should be ascribed to the hydrogen bonding and or ionic bonding during the LLPS.[41] Apart from the photostability and thermostability of MSPS materials, the material was degradable and highly recyclable. As the **ADM** macrocycle was synthesized by the linkage of disulfide bonds, it should be redox-responsive. With the addition of a 10 equiv biocompatible reductant dithiothreitol (DTT), a piece of bulk material processed from **ADM-4CTAB** MSPS materials, was first degraded into an orange homogeneous aqueous solution in 5 min. Then, the orange solution transformed into a colourless solution after 5 hours (Figure 4f). We reasoned that the reduction proceeded in two steps by analysing the $^1$H NMR spectra (Figure 4g, h). To facilitate comparative analysis, a homogeneous **ADM** (10 mM)/**CTAB**/1 : 5 aqueous solution was analysed rather than the insoluble **ADM-4CTAB** MSPS materials. In the first stage, the disulfide bonds of the **ADM** macrocycle were reduced to thiol groups.[17,42] The initial wide peaks of protons $m_1$ and $m_2$ were slightly split into sharp peaks, indicating the disassembly of MSPS aggregates. The proton signals of cysteine moieties shifted upfield due to the cleavage of adjacent disulfide bonds. In the second stage, the azobenzene groups were further reduced into diphenylhydrazine

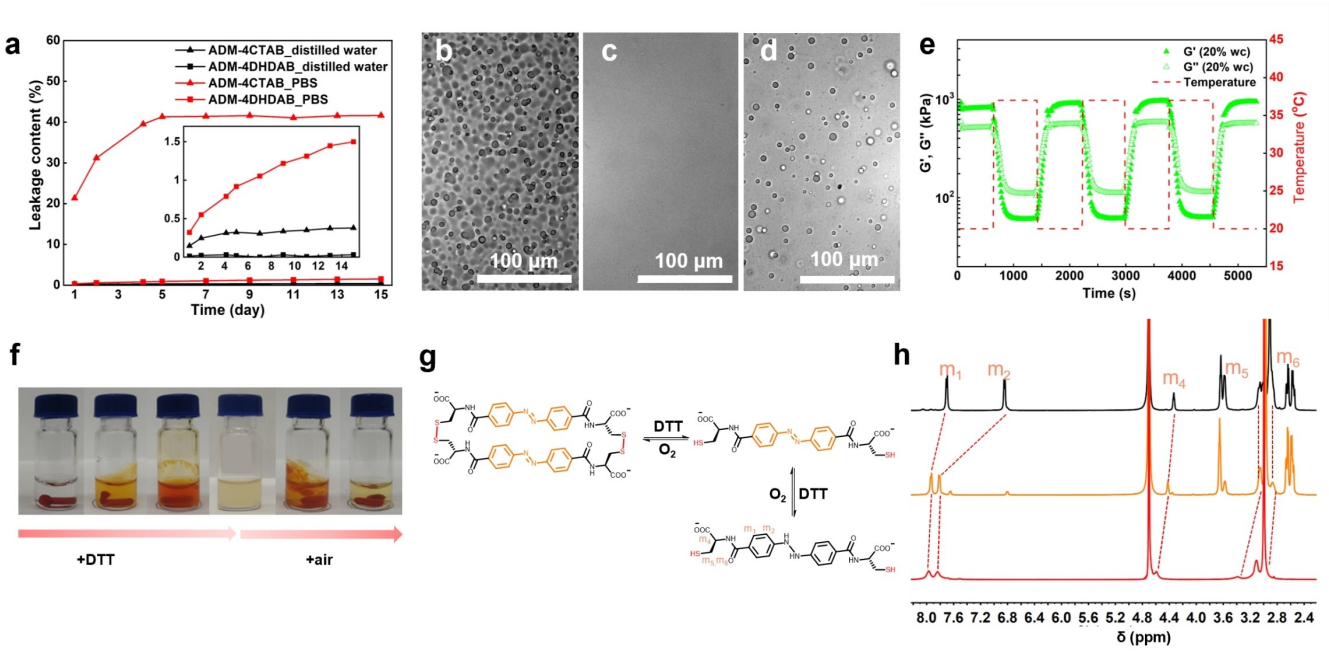


***Figure 4.*** a) Leakage content of **ADM-4CTAB** and **ADM-4DHDAB** MSPS materials in PBS solution (37 °C, shaker) and distilled water (room temperature). b)–d) Bright field microscopy images of **ADM-4CTAB** MSPS materials (b) before, (c) after UV 365 nm irradiation for 60 s, (d) after remove UV light and stay in dark for 5 min (1 mM, $H_2O$, pH 10, room temperature). e) Cyclic temperature sweep measurements of **ADM-4CTAB** MSPS materials with ≈20% water content. f) The appearance of a piece of bulk **ADM-4CTAB** MSPS materials reduction in water by adding 10 equiv DTT, and subsequent oxidation by loosening the cap in air. g) The chemical structure illustration of reversible redox of **ADM** macrocycle by DTT and oxygen. h) The contrastive $^1$H NMR spectrum of **ADM-4CTAB** MSPS materials after adding 10 equiv DTT, bottom: before adding DTT (replaced by **ADM** (10 mM)/**CTAB**/1 : 5 aqueous solution), medium: after adding DTT for 5 min, top: after adding DTT for 5 h ($D_2O$, 500 MHz, 10 mM for **ADM**, pD 10).

groups,[43,44] accompanied by the fading of solution colour, and protons $m_1$ and $m_2$ near the azobenzene bond significantly shifted upfield. The bulk MSPS material reformed after full oxidation in air overnight (Figure 4f). Similar to freshly prepared materials, the reformed materials could be easily separated from the solution, this process could be repeated for several times only with slightly (5%) weight loss (Figure S27) and the composition of the recycled material was unchanged, which was confirmed by $^1$H NMR (Figure S28). In addition, the MSPS materials were reusable due to their dynamic supramolecular structures. The MSPS materials used could be reshaped and reused through a simple process of reabsorbing water at room temperature. The adhesive strength of the material showed no obvious decreases even after reuse many times, and its mechanical properties remained the original strength after recycling many times (Figure S29). The $^1$H NMR spectra of recyclable MSPS materials further confirmed that the composition remained stable without any spoilage or degradation (Figure S30).

## Conclusion

We have demonstrated that LLPS could be an effective strategy for exploring supramolecular plastics with mechanical properties comparable to those of conventional covalent polymers without the loss of responsiveness. LLPS was triggered by the ionic interaction between an ionized macrocycle and an oppositely charged surfactant. The properties of the bulk MSPS materials were highly dependent on the water content inside the material. The initial material separated from the solution retained the most water content and featured fluidic properties. The material had instant self-healing properties and strong adhesive properties in air and underwater. By releasing water, the materials became gels with more solid-like characteristics. The water retention capacity of MSPS materials can be tuned by the hydrophobic proportion of surfactants, which can further exhibit a distinguishable function. Bulk MSPS materials made from macrocycles **ADM** and **CTAB** with a single alkyl tail surfactant showed excellent adhesive strength against hydrophilic substrates at high water contents. When the material was prepared from the same macrocycle and **DHDAB** with double alkyl tails, the resulting material had a weaker water retention ability but improved robustness and elongation properties. In addition, the MSPS materials showed highly dynamic and stimuli-responsive properties due to reversible supramolecular interactions and dynamic covalent bonding. The material had fully reversible thermal responsiveness and redox responsiveness and, more significantly, could be reusable and recyclable without obvious performance degradation for many cycles with mild and energy-saving procedures.

In summary, LLPS is usually caused by interactions involved by polymers. The structural complexity of macromolecules leads to our incomplete understanding of the phase separation phenomenon at the molecular level. Our study of MSPS materials formed by small molecules with much simpler structures should deepen the knowledge of the molecular interactions that give rise to LLPS. Our findings suggest that small molecule-based LLPS could be applied to construct supramolecular materials that are robust, adhesive, self-healable, degradable and highly recyclable, offering new ideas for the application of supramolecular polymers in practical fields in the future, such as recyclable plastics and smart soft materials.

## Acknowledgements

We are grateful for the financial support from the Sigrid Jusélius Foundation and the Academy of Finland (Decision No.318524). TEM imaging was performed in the Laboratory of Electron Microscopy, Institute of Biomedicine, the University of Turku, which receives financial support from Biocentre Finland. We thank Mr. C. Chen for performing preliminary experiments. We thank W. Liang (RWTH Aachen University, Germany) for her help with AFM measurements. We are grateful for Prof. S. Otto (University of Groningen, the Netherlands) for providing us the **ADM** for initial tests, Prof. D. Adams (University of Glasgow, GB) and anonymous reviewers for their insightful comments to the material.

## Conflict of Interest

The authors declare no conflict of interest.

## Data Availability Statement

The data that support the findings of this study are available from the corresponding author upon reasonable request.

**Keywords:** Electrostatic Self-Assembly · Liquid-Liquid Phase Separation · Macrocycles · Supramolecular Materials

[1] R. Geyer, J. R. Jambeck, K. L. Law, *Sci. Adv.* **2017**, *3*, e1700782.
[2] T. Aida, E. W. Meijer, S. I. Stupp, *Science* **2012**, *335*, 813–817.
[3] X. Z. Yan, F. Wang, B. Zheng, F. H. Huang, *Chem. Soc. Rev.* **2012**, *41*, 6042–6065.
[4] E. A. Appel, J. del Barrio, X. J. Loh, O. A. Scherman, *Chem. Soc. Rev.* **2012**, *41*, 6195–6214.
[5] A. Harada, Y. Takashima, M. Nakahata, *Acc. Chem. Res.* **2014**, *47*, 2128–2140.
[6] D. W. R. Balkenende, C. A. Monnier, G. L. Fiore, C. Weder, *Nat. Commun.* **2016**, *7*, 10995.
[7] T. Christoff-Tempesta, Y. Cho, D. Y. Kim, M. Geri, G. Lamour, A. J. Lew, X. B. Zuo, W. R. Lindemann, J. H. Ortony, *Nat. Nanotechnol.* **2021**, *16*, 447–454.
[8] B. J. Cafferty, I. Gallego, M. C. Chen, K. I. Farley, R. Eritja, N. V. Hud, *J. Am. Chem. Soc.* **2013**, *135*, 2447–2450.
[9] T. L. Price, H. W. Gibson, *J. Am. Chem. Soc.* **2018**, *140*, 4455–4465.

[10] Y. X. Deng, Q. Zhang, B. L. Feringa, H. Tian, D. H. Qu, *Angew. Chem. Int. Ed.* **2020**, *59*, 5278–5283; *Angew. Chem.* **2020**, *132*, 5316–5321.
[11] I. Michaeli, J. T. G. Overbeek, M. J. Voorn, *J. Polym. Sci.* **1957**, *23*, 443–450.
[12] N. A. Yewdall, A. A. M. Andre, T. M. Lu, E. Spruijt, *Curr. Opin. Colloid Interface Sci.* **2021**, *52*, 101416.
[13] C. E. Sing, S. L. Perry, *Soft Matter* **2020**, *16*, 2885–2914.
[14] A. Sorrenti, O. Illa, R. M. Ortuno, *Chem. Soc. Rev.* **2013**, *42*, 8200–8219.
[15] Q. Zhao, D. W. Lee, B. K. Ahn, S. Seo, Y. Kaufman, J. N. Israelachvili, J. H. Waite, *Nat. Mater.* **2016**, *15*, 407–412.
[16] M. Dompé, F. J. Cedano-Serrano, O. Heckert, N. van den Heuvel, J. van der Gucht, Y. Tran, D. Hourdet, C. Creton, M. Kamperman, *Adv. Mater.* **2019**, *31*, 1808179.
[17] J. W. Li, I. Cvrtila, M. Colomb-Delsuc, E. Otten, S. Otto, *Chem. Eur. J.* **2014**, *20*, 15709–15714.
[18] J. P. Douliez, N. Martin, C. Gaillard, T. Beneyton, J. C. Baret, S. Mann, L. Beven, *Angew. Chem. Int. Ed.* **2017**, *56*, 13689–13693; *Angew. Chem.* **2017**, *129*, 13877–13881.
[19] N. Martin, L. F. Tian, D. Spencer, A. Coutable-Pennarun, J. L. R. Anderson, S. Mann, *Angew. Chem. Int. Ed.* **2019**, *58*, 14594–14598; *Angew. Chem.* **2019**, *131*, 14736–14740.
[20] W. M. Aumiller, C. D. Keating, *Nat. Chem.* **2016**, *8*, 129–137.
[21] D. Priftis, M. Tirrell, *Soft Matter* **2012**, *8*, 9396–9405.
[22] E. Kizilay, A. B. Kayitmazer, P. L. Dubin, *Adv. Colloid Interface Sci.* **2011**, *167*, 24–37.
[23] D. Šmejkalová, A. Piccolo, *Environ. Sci. Technol.* **2008**, *42*, 699–706.
[24] M. C. T. Fyfe, J. F. Stoddart, *Coord. Chem. Rev.* **1999**, *183*, 139–155.
[25] R. Zhang, Y. P. Zhang, H. S. Antila, J. L. Lutkenhaus, M. Sammalkorpi, *J. Phys. Chem. B* **2017**, *121*, 322–333.
[26] J. Ostrowska-Czubenko, M. Gierszewska-Druzynska, *Carbohydr. Polym.* **2009**, *77*, 590–598.
[27] F. Müller-Plathe, *Macromolecules* **1998**, *31*, 6721–6723.
[28] Z. H. Ping, Q. T. Nguyen, S. M. Chen, J. Q. Zhou, Y. D. Ding, *Polymer* **2001**, *42*, 8461–8467.
[29] S. Y. Dong, J. Leng, Y. X. Feng, M. Liu, C. J. Stackhouse, A. Schonhals, L. Chiappisi, L. Y. Gao, W. Chen, J. Shang, L. Jin, Z. H. Qi, C. A. Schalley, *Sci. Adv.* **2017**, *3*, eaao0900.
[30] W. Dzwolak, A. Loksztejn, V. Smirnovas, *Biochemistry* **2006**, *45*, 8143–8151.
[31] M. Guvendiren, H. D. Lu, J. A. Burdick, *Soft Matter* **2012**, *8*, 260–272.
[32] S. T. Sun, L. B. Mao, Z. Y. Lei, S. H. Yu, H. Colfen, *Angew. Chem. Int. Ed.* **2016**, *55*, 11765–11769; *Angew. Chem.* **2016**, *128*, 11939–11943.
[33] C.-Y. Shi, Q. Zhang, H. Tian, D.-H. Qu, *Smart Mater. Struct.* **2020**, *1*, e1012.
[34] W. Zhao, J. Tropp, B. Qiao, M. Pink, J. D. Azoulay, A. H. Flood, *J. Am. Chem. Soc.* **2020**, *142*, 2579–2591.
[35] Q. Zhang, C. Y. Shi, D. H. Qu, Y. T. Long, B. Feringa, H. Tian, *Sci. Adv.* **2018**, *4*, eaat8192.
[36] A. H. Hofman, I. A. van Hees, J. Yang, M. Kamperman, *Adv. Mater.* **2018**, *30*, 1704640.
[37] T. L. Sun, T. Kurokawa, S. Kuroda, A. Bin Ihsan, T. Akasaki, K. Sato, M. A. Haque, T. Nakajima, J. P. Gong, *Nat. Mater.* **2013**, *12*, 932–937.
[38] X. Z. Yan, Z. Y. Liu, Q. H. Zhang, J. Lopez, H. Wang, H. C. Wu, S. M. Niu, H. P. Yan, S. H. Wang, T. Lei, J. H. Li, D. P. Qi, P. G. Huang, J. P. Huang, Y. Zhang, Y. Y. Wang, G. L. Li, J. B. H. Tok, X. D. Chen, Z. A. Bao, *J. Am. Chem. Soc.* **2018**, *140*, 5280–5289.
[39] D. Priftis, X. X. Xia, K. O. Margossian, S. L. Perry, L. Leon, J. Qin, J. J. de Pablo, M. Tirrell, *Macromolecules* **2014**, *47*, 3076–3085.
[40] W. J. Mu, Z. Ji, M. S. Zhou, J. Z. Wu, Y. Y. Lin, Y. Qiao, *Sci. Adv.* **2021**, *7*, eabf9000.
[41] O. Erol, A. Pantula, W. Liu, D. H. Gracias, *Adv. Mater. Technol.* **2019**, *4*, 1900043.
[42] M. Abbas, W. P. Lipinski, K. K. Nakashima, W. T. S. Huck, E. Spruijt, *Nat. Chem.* **2021**, *13*, 1046–1054.
[43] G. Zeyat, K. Ruck-Braun, *Beilstein J. Org. Chem.* **2012**, *8*, 890–896.
[44] A. D. Wong, T. M. Gungor, E. R. Gillies, *ACS Macro Lett.* **2014**, *3*, 1191–1195.

Manuscript received: March 29, 2022
Accepted manuscript online: August 5, 2022
Version of record online: August 24, 2022